Original Article

Zoledronate loaded polylactic acid/polycaprolactone/hydroxyapatite scaffold accelerates regeneration and led to enhance structural performance and functional ability of the radial bone defect in rat

Oryan, A.[1*]; Hassanajili, S.[2] and Sahvieh, S.[3]

[1]Department of Pathobiology, School of Veterinary Medicine, Shiraz University, Shiraz, Iran; [2]Department of Chemical Engineering, School of Chemical and Petroleum Engineering, Shiraz University, Shiraz, Iran; [3]Graduated from School of Veterinary Medicine, Shiraz University, Shiraz, Iran

*Correspondence: A. Oryan, Department of Pathobiology, School of Veterinary Medicine, Shiraz University, Shiraz, Iran. E-mail: oryan@shirazu.ac.ir

Abstract

Background: One of the most common concerns in the regeneration of massive bone defects necessitating surgery and bone grafts is the application of tissue engineering using drug delivery. Zoledronate is a well-known effective drug for the healing bone fractures in osteoporotic patients. **Aims:** An attempt was made to design a more efficient bone scaffold with polycaprolactone, polylactic acid, and hydroxyapatite. **Methods:** The scaffold was fabricated by freeze-drying and indirect 3D printing approaches. X-ray diffraction, Fourier transform infrared spectroscopy, rheometry, scanning electron microscopy, and neutral red tests were performed to characterize the scaffold. qRT-PCR was also done to define the osteoinductivity and angiogenic induction capacity of this scaffold. Forty rats were selected and randomly divided into four groups: the control group, which received no treatment, the autograft group, scaffold group, and Zol-loaded scaffold group (n=10 in each group). The injured area was studied by radiology, biomechanical analysis, histopathology, histomorphometry, immunohistochemistry, and CT scan analyses. **Results:** The qRT-PCR results demonstrated significantly higher expression levels of *OPN*, *OCN*, and *CD31* markers in the scaffold group when compared to the control group (P<0.05). Histopathologically, the newly formed bone tissue was significantly detected in the Zol-loaded scaffold and autograft groups in comparison with the non-treated group (P<0.001). The immunohistochemistry (OC marker), biomechanical, and histomorphometric results indicated a significant improvement in the regeneration of the injured area in the groups treated with autologous bone and Zol-loaded scaffold compared to the non-treated group (P<0.05). **Conclusion:** The Zol-loaded scaffold accelerated bone regeneration, and led to enhanced structural performance and functional ability of the injured radial bone in rats.

Key words: Bone regeneration, Critical bone defect, PLA/PCL/HA scaffold, Radius, Zoledronate

Introduction

Today, the main concern of orthopedic surgeons and investigators is to obtain a reliable method for enhancing bone regeneration with no or limited disadvantages. Some issues such as fractures and infections impair bone structure and function; therefore, bone tissue reconstruction and regeneration are extensively noticeable (Oryan *et al*., 2014a, b; Moshiri *et al*., 2015; Alidadi *et al*., 2017). Bone abnormalities such as trauma, osteotomies, bone tumor resections, osteomyelitis, compound or pathologic fractures, and chronic bone infections, which commonly give rise to massive bone defects, require treatment and reconstruction, using effective methodologies (Oryan *et al*., 2014a, b). In a qualified bone regeneration process, the defected area is regenerated by a well vascularized bone-like tissue resulting in adequate stability and proper skeletal function (Mathavan *et al*., 2013; Kyllonen *et al*., 2015; Sahvieh *et al*., 2021). Some regulated signaling pathways have vital roles in bone regeneration via balancing the catabolic and anabolic processes. Manipulating the anabolic and catabolic phases by biological, pharmacological, and mechanical interventions results in a more efficient bone regeneration procedure (Mathavan *et al*., 2013).

The role of a complex set of regulated signaling pathways has been found notable in bone repair. In fact, the role of these signaling pathways is to reabsorb the damaged bone matrix and control the synthesis of the new bone matrix. These pathways are primarily initiated by balanced anabolic and catabolic responses in which

the osteoblasts are responsible in new bone formation, and the osteoclasts resorb the original bone. When the balance is disturbed, because of the increased catabolic or failure in anabolic responses or both, the healing process may be disrupted and thus the delayed union or non-union may occur (Doi *et al*., 2011).

Tissue engineering is a promising modality for tissue regeneration and reconstruction and all the constituents used in this method are effective in the regeneration and repair of the defected area (Oryan *et al*., 2020). Application of biomaterials such as alginate/ hydroxyapatite, poly (lactide) (PLA), chitosan, poly (ε-caprolactone), gelatin poly (glycolic acid), and polylactide-co-glycolide (PLGA) is the crucial part of tissue engineering. These biomaterials are characterized and used as bone grafts, due to their osteogenic-enhancing ability, biocompatibility, adjustable pore conformation, non-antigenicity, biodegradability, and non-cytotoxicity. They can also enhance cell proliferation, cell differentiation, and attachment resulting in improved bone regeneration (Oryan *et al*., 2014a; Witzler *et al*., 2019; Yu *et al*., 2019). Furthermore, drug delivery has been considered the most efficient and cost-effective method when accompanied by tissue engineering based on biocompatibility, non-cytotoxicity, cytocompatibility, non-allergenicity, anti-microbial, and bioactivity (Oryan *et al*., 2017).

Both polylactic acid (PLA) and polycaprolactone (PCL) are the most investigated polyesters which are widely utilized in reconstructive medicine. These biocomposites have been approved by the United States Food and Drug Administration Office due to their beneficial properties such as thermal transition ability, mechanical strength features, crystallinity, and ease of processing (Washington *et al*., 2017). Hydroxyapatite (HA) is a natural biocomposite that is suitable for bone tissue engineering because its structure resembles bone tissue (Sahvieh *et al*., 2021). In undertaking the present study, a new operational scaffold, fabricated with three different materials including HA, PCL, and PLA, was designed. The scaffold has some unique characteristics such as biodegradability, crystallinity, and bio-compatibility for the HA constituent. HA has also a suitable character for bone tissue, which leads to new bone formation, hence reducing the duration of healing (Eftekhari *et al*., 2018; Kumar *et al*., 2018). The PLA counterpart is a useful constituent in manufacturing a weight-bearing bone scaffold due to its 90% porosity, the establishment of a proper environment for cell ingrowth, thermal plasticity, biocompatibility, nutrient distribution, and characteristic positive mechanical behavior. In addition, this material is biodegradable by lactic acid, which normally exists in the body tissues (Lopes *et al*., 2012; Gregor *et al*., 2017). The features related to the PCL include mechanical strength, workability, biocompatibility, and bioabsorbability. Similar to the PLA counterpart, PCL also degrades into harmless/non-toxic by-products (Eftekhari *et al*., 2018).

Zoledronate (Zol) is a nitrogen containing bisphosphonate (BP) that is able to prevent the migrating and differentiating of the osteoclast precursors to the inflammatory osteolytic lesions, producing an inhibitory effect on bone mass mature osteoclasts (Senel *et al*., 2010; Lim *et al*., 2017). BPs are coated on orthopedic implants, and result in the acceleration of fracture healing, increasing the mechanical fixation of implants, improving the stability of joint replacements, and upgrading fixation and the bone volume surrounding the screws (Ortega *et al*., 2012). The effects of Zol on bone healing also include improvement in mineralization, the recruitment and proliferation of osteoblast-like cells, and remodeling (Matos *et al*., 2010; Roshan-Ghias *et al*., 2011; Yu *et al*., 2012; Kettenberger *et al*., 2014). It has been reported that Zoledronate enhanced the mechanical strength of regenerated femoral defect (Doi *et al*., 2011), and its low dose could develop new bone formation when it was utilized as a local delivery route (Ma *et al*., 2018). When Zoledronate was incorporated into poly L, D lactic acid (PDLLA), it improved fracture healing, and resulted in greater mechanical strength and callus area, and improved the speeds of fracture bridging in the closed tibial fracture of rats (Greiner *et al*., 2008).

The fabrication of the scaffold was performed by freeze-drying and 3D printing methods as previously reported by Hassanajili *et al*. (2019). According to these approaches, cell proliferation and adherence waere improved *in vitro* (Hassanajili *et al*., 2019). The porous 3D scaffold accompanied by suitable micro- and macro-pores creates sufficient angiogenesis. In fact, porogen leaching, salt leaching, direct/indirect 3D printing, electrospinning, and hydrogel techniques are the most known approaches to creating a porous scaffold. The indirect 3D printing method that was used to fabricate our scaffold provided the macro-structural properties during a negative mold preparation and also allowed the designing of the scaffold to match the defect geometry of the patient. By this method, the porosity and pore size of the final scaffold was controllable and was notable in providing a prime environment for cell migration and growth. Besides, the freeze-drying method allowed the production of microporous structures when it was used following solution casting in the negative mold (Frydrych and Chen, 2013; Babczyk *et al*., 2014; Chen *et al*., 2014; Do *et al*., 2015; Ottensmeyer *et al*., 2018; Gotz *et al*., 2019).

The current study aimed to demonstrate the ability of 50-50-35% PLA/PCL/HA scaffold fabricated via the combination of the freeze-drying method with indirect 3D printing. The scaffold was fabricated and characterized by X-ray diffraction, Fourier transform infrared spectroscopy, rheometry, scanning electron microscopy, and neutral red methodologies. More specifically, the potential of Zol-loaded PLA/PCL/HA on the regeneration of a critical-sized defect of radius in rats was investigated. This experimental study was conducted using gross pathology, radiology, biomechanical analysis, histopathology, histomorphometry, immuno-histochemistry, and CT scan analyses to determine the best approach to forming a new bone structure.

Materials and Methods

Chemicals and preparation of the PCL/PLA/HA scaffold

PLA (molecular weight = 120,000), PCL (molecular weight = 70,000-90,000), HA (particles of 100 nm in diameter), D-Fructose, and 99.8% chloroform were sourced from MG Chemicals, Sigma Aldrich, and Merck Co. Before fabricating the scaffold by 3D printing (ZMorph Co., 0.3 mm nozzle size) and freeze-drying methods, all materials were dried for 24 h in a vacuum oven, and then PLA, PCL, fructose, and HA were mixed into chloroform and stirred at room temperature in cord with the Hassanajili *et al*. (2019) procedure (Fig. 1).

Characterization of the scaffold

The morphology and structure of the scaffold were observed by a TESCAN-Vega 3 scanning electron microscope. As HA was used in the fabrication of the scaffold, the elemental analysis was determined by energy-dispersive X-ray spectroscopy. Fluid displacement was used to measure the porosity via immersion of the scaffold in ethanol. The compression test (Zwick/roll apparatus) on a 2×1 cm^2 cubic piece of the scaffold resulted in the mechanical features and a rheometer (Physica MCR 302, Anton Paar, Austria) measured the rheological behaviors such as complex viscosity and dynamic functions. Based on the degradation pattern of this scaffold, 0.01 M phosphate-buffered saline was utilized at five different time intervals and the pH values were then assessed. X-ray diffraction was performed at room temperature to ascertain the crystallinity of the PCL, HA, and PLA counterparts by Bruker D8 Advance apparatus to achieve data from 2Ө range of 10-80° (interval = 0.05°). Fourier transformer infrared spectroscopy was also used to understand the molecular interaction and scaffold function (NEXUS670 FTIR spectrometer by 4000-400 cm^{-1} wavenumber) (Hassanajili *et al*., 2019).

The human umbilical cord mesenchymal stem cell line, provided by Royan Institute (Tehran, Iran) was seeded on the top surface of the scaffold to understand the morphological features of the adhered cells basis on the SEM images and cell viability through a neutral red test guided by Oryan *et al*. (2020) investigation.

Loading Zoledronate onto the scaffold

In line with the results of the Boanini *et al*. (2014) study, 7 µM of the Zoledronate drug (SML0223, Sigma) was loaded onto the scaffold (sterilized by 70% alcohol and UV light) which was implanted onto the defect site.

In vivo study

In vivo study was also performed similarly to Oryan *et al*. (2020). Briefly, forty adult male Wister rats (225 g ± 25) were divided into four groups: control (untreated defect), autograft, scaffold, and Zol-loaded scaffold groups (n=10 in each group). The animals were housed five days before the start of study for acclimatization [(humidity = 30-0%, temperature = 19-6°C, lighting = 300 lux, 12:2 light: dark cycle), with the rat maintenance food and water *ad libitum*] in $59 \times 38.5 \times 30$ cm cages in groups of four. This experimental study was approved by the Ethics Committee for the use of animals in the scientific procedures of the School of Veterinary Medicine of Shiraz University. The rats gained humane care, which followed the Guide for Care and Use of Laboratory Animals published by the National Institutes of Health (NIH Publication No. 85-23). The 5 mm defect was created by an electrical bone saw that was purchased from Strong Company (Seoul, South Korea). The intact ulnar bone was a protector of the defected radius.

Real-time RT-PCR (qRT-PCR) analysis

The osteogenesis potential of the scaffold was determined by *OCN* and *OPN* gene expression analysis. *CD31* gene expression was measured to determine the angiogenesis potential of this scaffold according to the qRT-PCR results at 21 days post-seeding (Oryan *et al*., 2020) (Fig. 2). The samples were gathered from three biological replicates, and the ΔΔCT method was utilized to quantify gene expression. The *GAPDH* gene was used
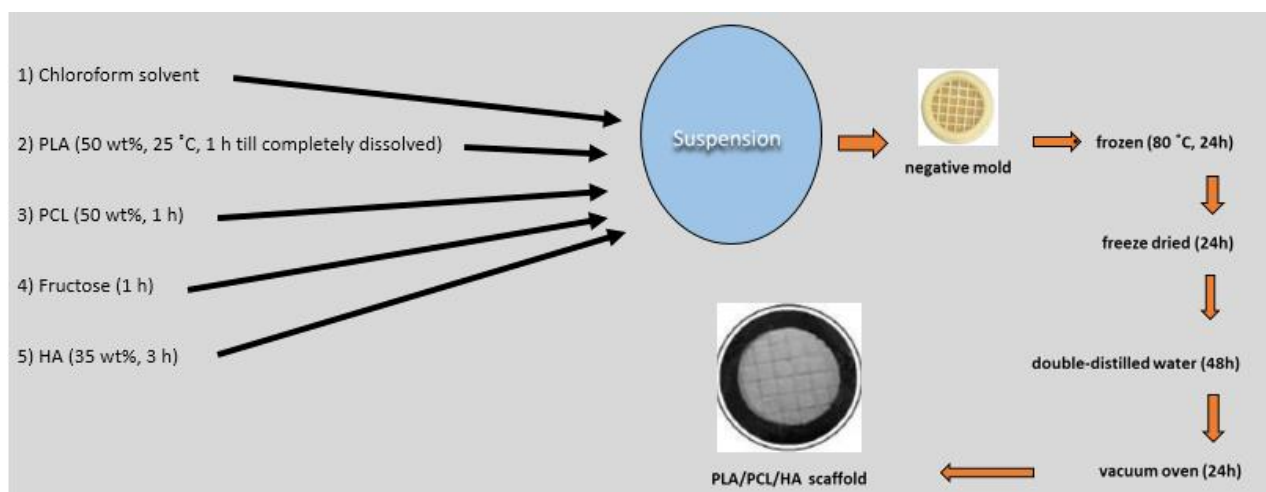

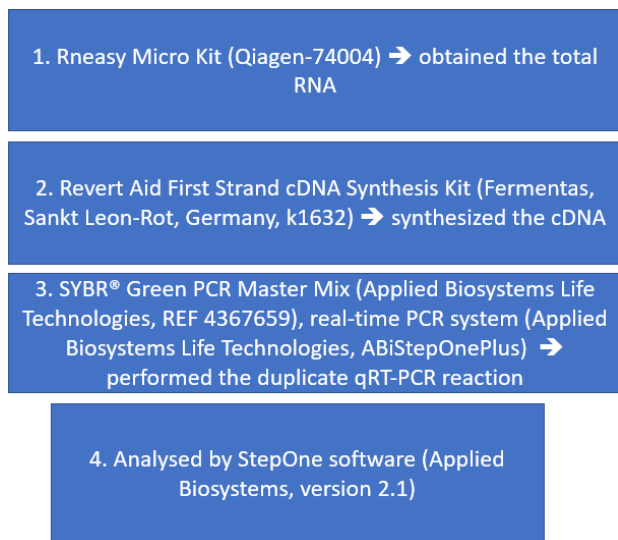**Fig. 1:** The process of fabricating PLA/PCL/HA scaffold

1. Rneasy Micro Kit (Qiagen-74004) ➔ obtained the total RNA

2. Revert Aid First Strand cDNA Synthesis Kit (Fermentas, Sankt Leon-Rot, Germany, k1632) ➔ synthesized the cDNA

3. SYBR® Green PCR Master Mix (Applied Biosystems Life Technologies, REF 4367659), real-time PCR system (Applied Biosystems Life Technologies, ABiStepOnePlus) ➔ performed the duplicate qRT-PCR reaction

4. Analysed by StepOne software (Applied Biosystems, version 2.1)

Fig. 2: The phases of the qRT-PCR analysis, kits, and software

as the normalizer gene, and the control group was assumed as the calibrator group in the ΔΔCT analysis.

Computed tomography, gross pathology, and radiological evaluations

The animals were anesthetized, and the radiographs were taken from the defect area of the radial bones, at the 40th and 80th days post-surgery, to analyze the rate of gap closure. The animals were then euthanized, and the harvested radial bones were used for macroscopic evaluation and CT scanning. The extent of the regenerated area was evaluated for gross pathology scoring (non-union defect = 0, incomplete union + fibrous connective tissue = +1, incomplete union + cartilage tissue = +2, and complete union + bridging bone = +3) (Oryan *et al*., 2012, 2020).

Histopathologic, histomorphometric, and immunohistochemical (IHC) analysis

After dissecting the radius bones from soft tissues and muscles and fixing them in neutral buffered formalin, decalcification was done by 14% EDTA, pH = 7.4, for 30 days, and the 5 µm sections were prepared from the paraffin blocks. The sections were stained with hematoxylin and eosin (H&E), and the histomorphometric analysis was conducted to obtain the cell count of fibroblasts, fibrocytes, chondroblasts, chondrocytes, osteoblasts, osteocytes, and osteoclasts along with inflammatory cells including neutrophils, macrophages, and lymphocytes. The number of blood vessels and the density of fibrous connective tissue, cartilage, and bone ingrowth were also assessed by the computer software Image-Pro Plus® V.6 (magnification ×400). The cell count was performed on six different microscopic fields, and the average of different indices was recorded. By detecting the osteocalcin (ab13420, Abcam, MA) and CD31 (ab119339, Abcam, MA) markers on day 80 post-surgery, the regeneration

potential of the scaffold and Zol-loaded scaffold was evaluated. After citrate buffer incubation overnight (60°C), the slides were blocked by hydrogen-peroxide ethanol (1% concentration). Following the incubation of slides at 4°C with markers (overnight), the color reaction was developed by 3, 3´-diaminobenzidine, and then hematoxylin counterstaining (Oryan *et al*., 2020).

Biomechanical analysis

The radial bones were collected after euthanasia, and were frozen after being wrapped into sterile moist gauzes at -20°C to find the biomechanical properties, including maximum load (N), stiffness (N/mm), ultimate strain (%), and ultimate stress (N/mm^2). The testing machine was a universal tensile testing instrument from Instron Co. (London, UK), and the strain rate was 5 mm/min (Oryan *et al*., 2020).

Statistical analysis

The one-way analysis of variance was performed for the quantitative data followed by the Turkey post hoc test. The Kruskal-Wallis and non-parametric ANOVA procedures were also run for the statistical analysis of the qualitative data. The Mann-Whitney U-test was conducted to assess the possibility of any significant differences among the groups of interest ($P<0.05$). The analytical diagrams from the data were drawn by Graph Pad Prism software (ver. 8.2.1).

Results

Structural features of the scaffold

As shown in Figs. 3a and b, the SEM ultra micrographs demonstrated sufficient porosity, macro-pores, micro-pores, optimal pore-interconnectivity, and pore size, which facilitated cell migration and nutrient transmission. The cells adhered strongly to the fabricated scaffold by their pseudopodia, at one-day post-seeding (Figs. 3a and b). The average diameter of micro-pores and thickness of pore walls were 141.01 ± 48.25 µm and 27.51 ± 2.94 µm, respectively.

The results of the elemental analysis that are shown in Fig. 4a suggest that the scaffold structure was similar to the bone tissue texture due to the presence of the HA particles in the implant. Based on these results, it is inferred that the C, Ca, P, and O were present in many parts of our scaffold, with a Ca to P ratio of 1.7. The average percentage of PLA/PCL/HA scaffold porosity was found to be in the range of 69-71%. The results of the compression test were diagramed in the stress-strain figure involving three stages of elastic response until 20% strain; pores collapse from pressure (20-40% strain), and densification of PLA/PCL/HA scaffold (45% strain) [compressive modulus (MPa) mean=0.6339 ± 0.03995] (Fig. 4b). The rheological results, based upon the analysis of SEM ultra micrographs of the PLA, PLA/PCL (50/50), and PCL are illustrated in Fig. 4c.
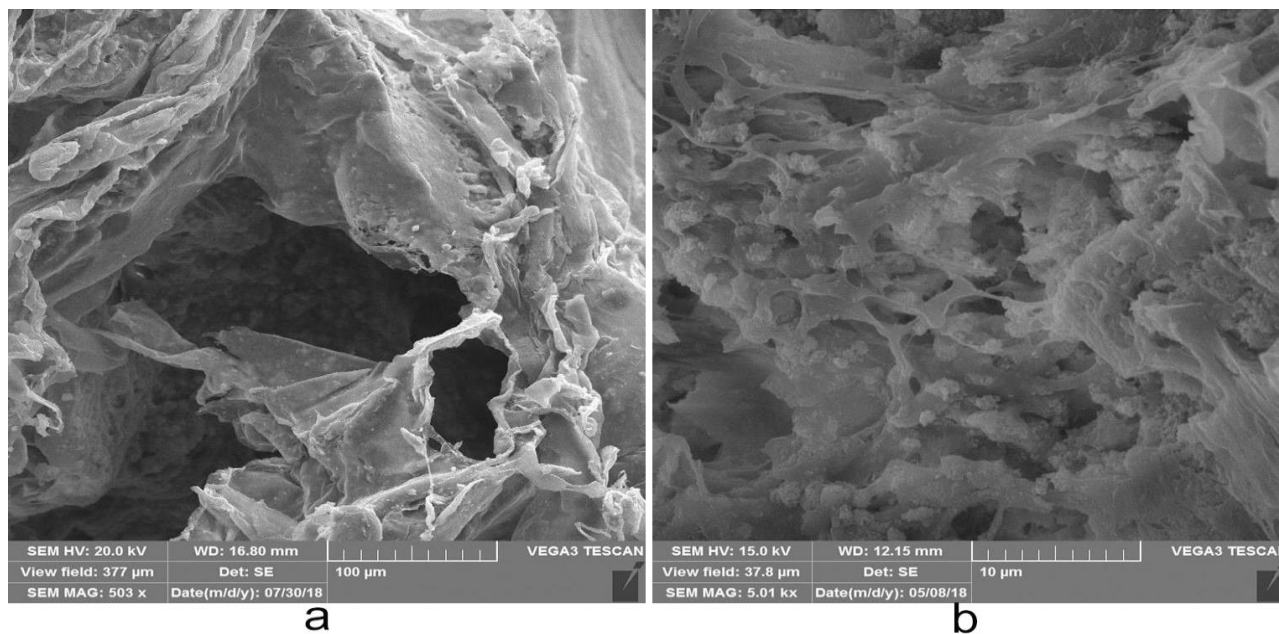
Fig. 3: The SEM ultra micrographs of the fabricated scaffold show the micro- and macro-porous structure of this bone implant. The image on the left side (**a**) shows the cell-free PLA/PCL/HA scaffold structure, and the one in the right side (**b**) shows the cell-seeded scaffold

The changes in degradation behavior can be accounted for by factors such as hydrophilicity, porosity, and microstructure. By releasing ions from the scaffold, its material degradation, and weight loss were identified. As it has been shown in Fig. 4d, the scaffold was degraded by 2-2.5% in the body pH, at the 35th day of implantation, pointing to a good possibility for bone tissue cells to migrate to the defect area. The established buffered behavior, due to the HA nanoparticles, is shown in Fig. 4e. It represents that the release of alkaline ions, resulted in an alkaline pH, and the acidic pH is accredited to the release of the polymer acidic by-products.

The XRD diagram (Fig. 4f) shows that the PCL caused more crystallinity than PLA. The peaks of the scaffold characteristic were related to HA, and the broadness and weak intensity were due to PLA phase HA sample represented diffraction peaks at 26°, 31.8°, 32.9°, 40°, and 49° and lattice parameters: at a=0.943 nm, b=0.493 nm, and c=0.688 nm. The PCL and PLA samples showed major diffraction peaks at $2\theta=16.6°$ and $2\theta=18.9°$ respectively, and lattice parameters at a=0.948 nm, b=0.498 nm, and c=1.727 nm. The reflections at $2\theta=21.6°$ and $2\theta=23.8°$ for the PCL and PLA samples were similar to polyethylene (orthorhombic) by the lattice morphology. The IR analysis was done for the PLA, HA, PCL, and PLA/PCL/HA samples [FTIR spectrum; PCL (CH_2 symmetric stretch at 2940 cm^{-1}, C-O stretch at 1160 cm^{-1}, carbonyl stretch at 1720 cm^{-1}, and CH_2 asymmetric stretch at 2860 cm^{-1}), PLA (carbonyl stretch band at 1740 cm^{-1}, CH_3 stretch band at 2883 cm^{-1}, and C-O stretch at 1032 cm^{-1}), HA (OH stretch peak at 3500 cm^{-1} and $PO4^{-3}$ stretch band around 1036 cm^{-1}), and all the peak positions are depicted in Fig. 4g. There are some shifts that are in peak position (e.g., carbonyl and hydroxyl groups) in comparison to the bands in the PLA/PCL/HA spectrum.

The neutral red test was performed to record cell viability in the cultures to depict the average optical density which was as follows: 1.29769 ± 0.15241 on day 3, 1.28952 ± 0.35146 on day 7, and 1.53146 ± 0.18214 on day 10.

qRT-PCR analysis

The expression level of the angiogenic and osteogenic-related genes by qRT-PCR, on the 21st day post-seeding, are represented in Fig. 5. There was a significantly higher expression level of OPN (P<0.01) and OCN (P<0.001) in the scaffold group compared to the control group. The PLA/PCL/HA scaffold group had also a significantly higher level of CD31 than the control group (P<0.05).

Clinical evaluation

Abnormal clinical signs, toxemia, and wound complication were not observed. Moderate to severe signs of pain and edema existed in the scaffold group, and mild to moderate pain and swelling was diagnosed in the Zol-loaded scaffold group. The inflammatory signs diminished in all groups on the 28th post-operation day. The weight-bearing and physical activity were normal in all rats due to the intact ulna.

Gross pathology

The new tissue, with a variable range of soft to hard connective tissues, filled the defect, and the scoring was recorded accordingly on the 40th and 80th days post-surgery (Table 1). Besides, the defect region in the control group was replaced by fibrous connective tissue or remained empty (Figs. 6a-z). The defect site of the scaffold group was supplied by cartilaginous like and
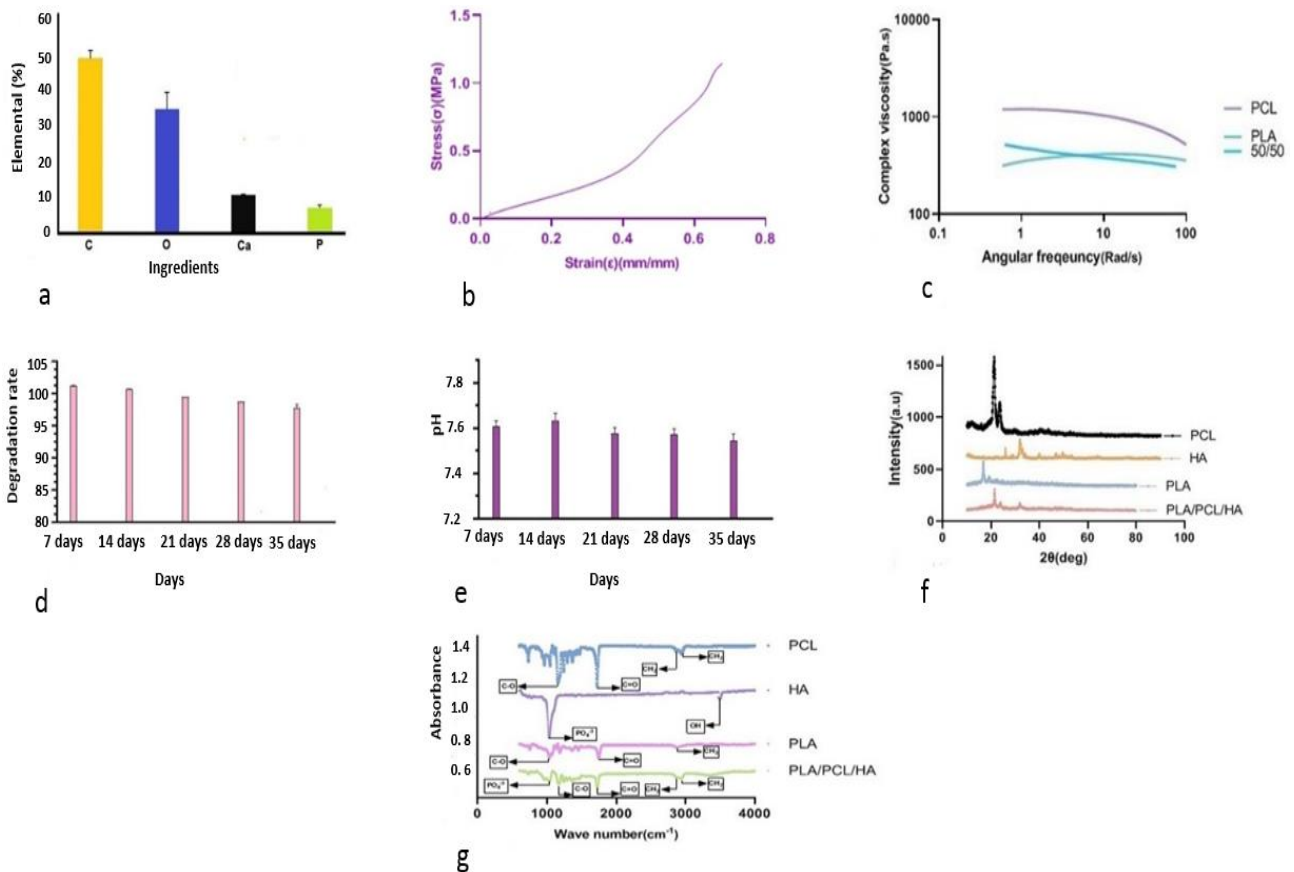
Fig. 4: The diagrams of scaffold's characteristics. (**a**) Elemental analysis of the PLA/PCL/HA scaffold, (**b**) Stress-strain diagram, (**c**) The complex viscosity-angular frequency diagram, (**d**) The degradation rate of PLA/PCL/HA scaffold at 7, 14, 21, 28, and 35 days, (**e**) The pH changes of the PLA/PCL/HA scaffold at 7, 14, 21, 28, and 35 days, (**f**) XRD pattern of the PCL/PLA/HA, PCL, PLA portions, and HA nanopowder, and (**g**) FTIR diagram of the PCL/PLA/HA, PCL, PLA, and HA Nanopowder

Table 1: Complete union by bonny tissue (+3 score), presence of cartilage (+2 score), presence of soft connective tissue (+1 score), and nonunion (0 score)

Group	Macroscopic score (day 40) Median (min-max)	Macroscopic score (day 80) Median (min-max)
Untreated defect (1)	0 (0-0)	1 (0-1)
Autograft (2)	2 (1-2)	3 (2-3)
Scaffold (3)	1 (1-2)	2 (1-2)
Scaffold + Zol (4)	2 (1-2)	3 (2-3)

Day 40: $P<0.01$ (2 *vs.* 4), and $P<0.05$ (1 *vs.* 3), and Day 80: $P<0.01$ (2 *vs.* 4), and $P<0.05$ (1 *vs.* 3) (Kruskal-Wallis Non-parametric ANOVA)
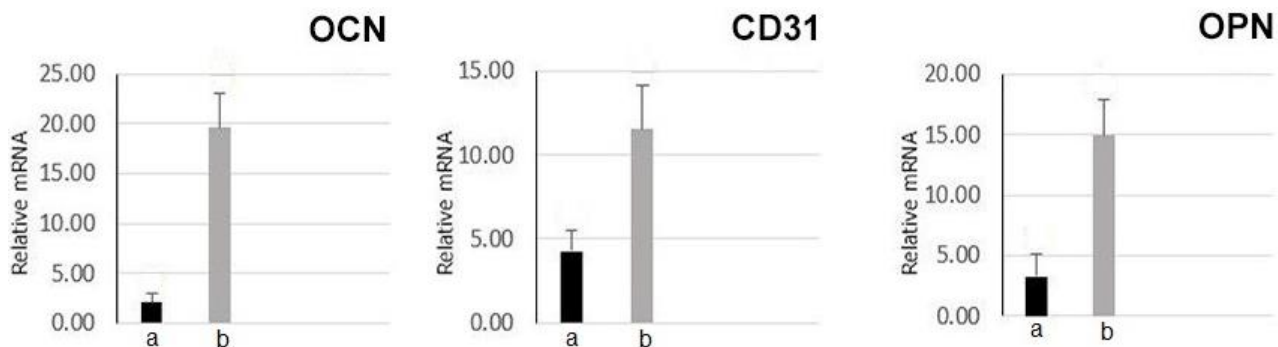

Fig. 5: The qRT-PCR analysis shows the expression level of osteogenic and angiogenic genes (*OCN*, *OPN*, and *CD31*) after 21 day. Promotion in the expression level of all these markers was observed in the scaffold group compared to the control group. *CD31*: $P<0.05$, *OCN*: $P<0.001$, and *OPN*: $P<0.01$. a: Control, and b: Scaffold
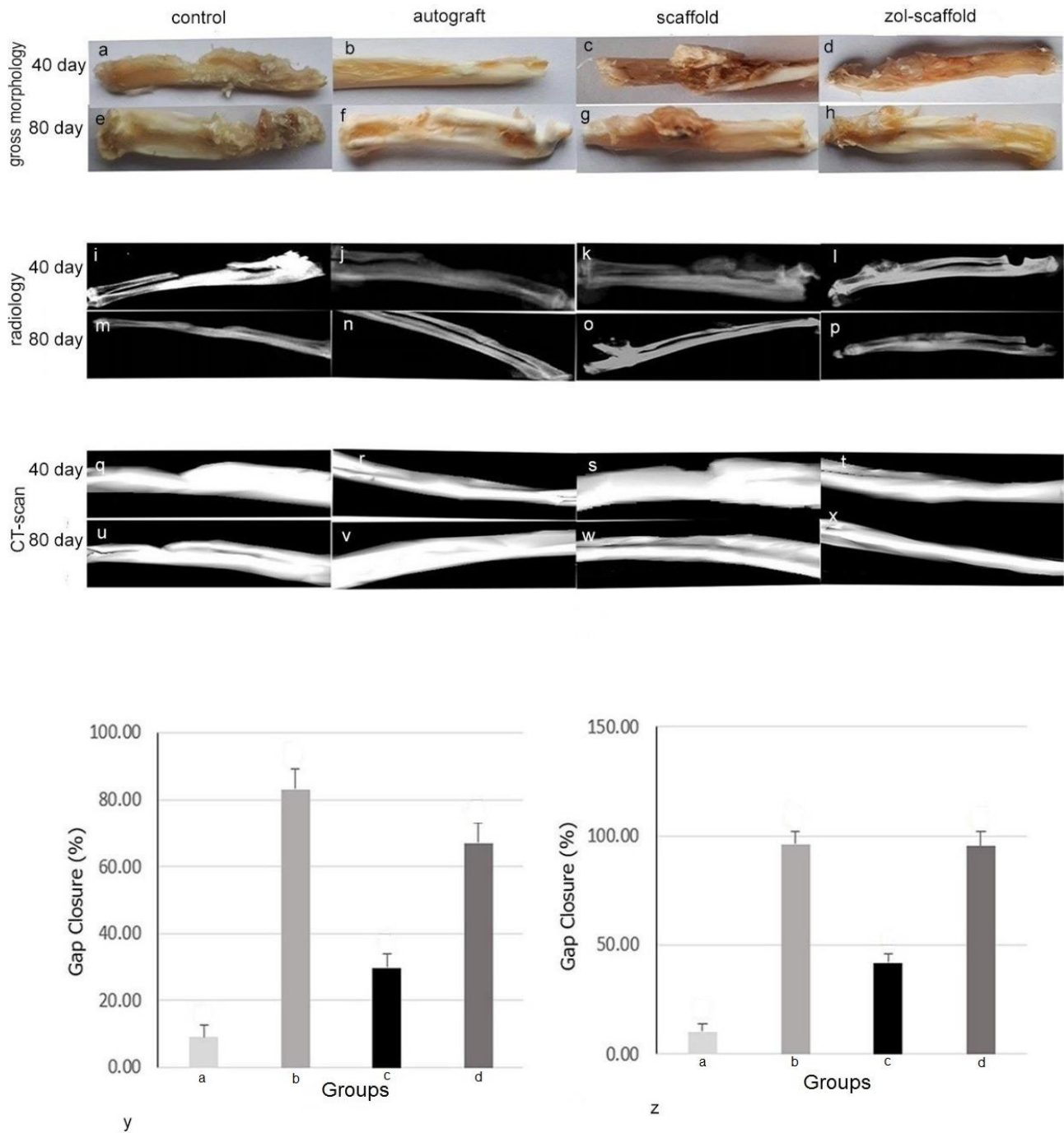
Fig. 6: The radiologic and gross pathology figures of the defect area on the 40th and 80th days post-injury. Residues of the scaffold were seen on the 40th day post-injury, in the scaffold group. (**y, z**) The rate of gap closure (%) in all treated and untreated groups. a: Control, b: Autograft, c: PLA/PCL/HA scaffold, and d: Zol-loaded scaffold. 40 days (**y**): a *vs.* c: P<0.05, c *vs.* d: P<0.01, a *vs.* d: P<0.001. 80 days (**z**): a *vs.* c: P<0.01, a *vs.* d: P<0.001

Table 2: Histomorphometric analysis of the defect area on the 80th day post-operation

Values	Mean±SD					
	FB±FC	CB±CC	OB±OC	Osteoclast	Osteon	Blood vessels
Untreated defect (1)	178.15±21.69	8.86±2.3	6.92±0.51	0	0	13.87±4.52
Autograft (2)	7.93±1.24	28.01±2.11	220.5±21.79	3.36±1.25	6±0.84	5.1±1.44
PLA/PCL/HA (3)	15.2±5.11	22.52±2.65	171.32±3.54	1.04±0.99	4.21±1.3	6.97±2.29
Zol-PLA/PCL/HA (4)	8.7±4.5	26.76±3.51	199±16.21	2.89±1.5	5±1.7	5.2±1.71

One-way ANOVA followed by Tukey post hoc test. FB: Fibroblast, FC: Fibrocyte, CB: Chondroblast, CC: Chondrocyte, OB: Osteoblast, and OC: Osteocyte [P<0.01 (1 *vs.* 2, 3, 4), and P<0.05 (2 *vs.* 3)]

fibrous connective tissues. However, in the Zol-loaded scaffold and autograft groups it was observed that a bony like tissue filled the defect region. The highest scores were detected in the autograft and Zol-loaded scaffold groups when compared to the untreated group (P<0.01). A significant difference was not detected between the Zol-loaded scaffold and autograft groups (P>0.05), albeit there was a significant difference between the scaffold and control groups (P<0.05).

Results of the diagnostic imaging

The rate of defect closure (%) was measured and analyzed on the 40th and 80th day post-surgery, using digital radiography. The evaluation demonstrated significant differences in the Zol-loaded scaffold and control groups (P<0.001) and also between the scaffold group and the non-treated group (P<0.05) (Figs. 6a-z).

Histopathologic and histomorphometric results

The least amount of bone regeneration was observed in the control group, where the closure of the defect was filled by collagen fibers, and fibrous or loose areolar connective tissue. Numerous fibroblasts, fibrocytes and newly formed blood vessels were present on the 40th day post-injury (Figs. 7a-h), and a ridge of fibrocartilage tissue at the edges of bones and fibrous connective tissue occupying the middle portion of the lesion was detected on the 80th day post-surgery in the control group (Figs. 8a-h). The defect area was completely filled by fibrovascular tissue and just a few chondrocytes and chondroblasts, and no osteoblasts were seen in the defect of the animals of this group on the 80th day post-injury (Figs. 8a-h). Osseointegration was observed at the edges of four out of the five bone samples of each of the autograft and Zol-loaded scaffold groups on day 40 post-injury. The defect was replaced by hyaline cartilage, fibrocartilage, and newly woven bone on the 80th day post-operation. The scaffold in the scaffold-treated gap was almost degraded after 80 days, and the gap was filled by a small amount of fibrous connective tissue, new hyaline cartilage, and more woven bone, especially at the edges of the original bones. The residue of the scaffold was encapsulated by fibrous connective tissue on the 40th day post-surgery. A successfully remodeled compact bone was seen in the Zol-loaded scaffold and autograft groups on the 80th day post-surgery.

The histomorphometric analysis demonstrated that the highest fibrocyte and fibroblast counts (Table 2) belonged to the control group compared to other treated groups on the 80th day post-surgery (P<0.05). However, the least osteoblast, chondrocyte, and chondroblast counts were also seen in this group. There were significant differences between the control group and the scaffold (P<0.05), and Zol-loaded scaffold (P<0.01) groups in the number of osteocytes, osteoblasts, and the density of osseous tissue. Finally, our experiment demonstrated that the capacity of new bone formation did not indicate a significant difference between the autograft and Zol-loaded scaffold groups (P>0.05) and that the PLA/PCL/HA scaffold group had a significant

difference with the untreated group (P<0.05).

Immunohistochemical (IHC) findings

The OC expression level was significantly higher in the scaffold and ZOL-loaded scaffold groups when compared to the untreated group (P<0.01) (Figs. 9a-h). The CD31 expression level also demonstrated a significant up-regulation in the scaffold and Zol-loaded scaffold groups in comparison to the control group (P<0.05). In fact, the defect in the control group depicted a lower level of these two markers.

Biomechanical findings

The treated groups significantly demonstrated the largest amount of maximum load (N), stiffness (N/mm), and stress (N/mm^2), compared to the non-treated group (P<0.01). The strain (%) was also significantly higher in the control group in comparison to the scaffold, Zol-loaded scaffold, and autograft groups (P<0.001) (Figs. 10a-d).

Discussion

Bone formation is referred to as an anabolic response but bone reabsorption is known as a catabolic reaction. Although both are necessary processes in bone healing. The first step in bone healing is characterized by endochondral ossification, which produces non-mineralized cartilage. Remodeling starts with the new lamellar bone formation following osteoclastic bone reabsorption (Matos *et al.*, 2010). It has been indicated that the PLA/PCL/HA scaffold has remarkable potential in developing bone regeneration by the superior ability of osteoinduction of its components (Grandi *et al.*, 2016; Mondal *et al.*, 2016; Gregor *et al.*, 2017). It has been shown that migration of the osteoblasts is developed due to the scaffold porosity and the existence of the HA particles, which results in enhanced bone healing (Shahsavari-Pour *et al.*, 2018; Fang *et al.*, 2019). By an indirect 3D printing approach, the shape of the scaffold could be designed with the feature that fixes both bone tissue defects and controls the micro- and macro-porous structure of the scaffold. Because of its degradation rate, physical features, and mechanical behavior, this fabricated scaffold has a favorable impression on osteoblast viability and calcium deposition. The highest degradation rate was observed in relation to the PLA, while the PCL ingredient reduced the rate of degradation. In fact, the presence of abundant and uniform pores in the scaffold led to the consistent distribution of the cells throughout the scaffold.

The results of the stress-strain diagram depicted all three stages based on our previous study (Hassanajili *et al.*, 2019). The first portion of this diagram demonstrated a linear response, while the second phase indicated the collapse of the pores after pressure tolerance. Finally, the third phase illustrated the results of scaffold densification. Based upon the shear-thinning behavior in the rheology analysis, the arrangement of the samples
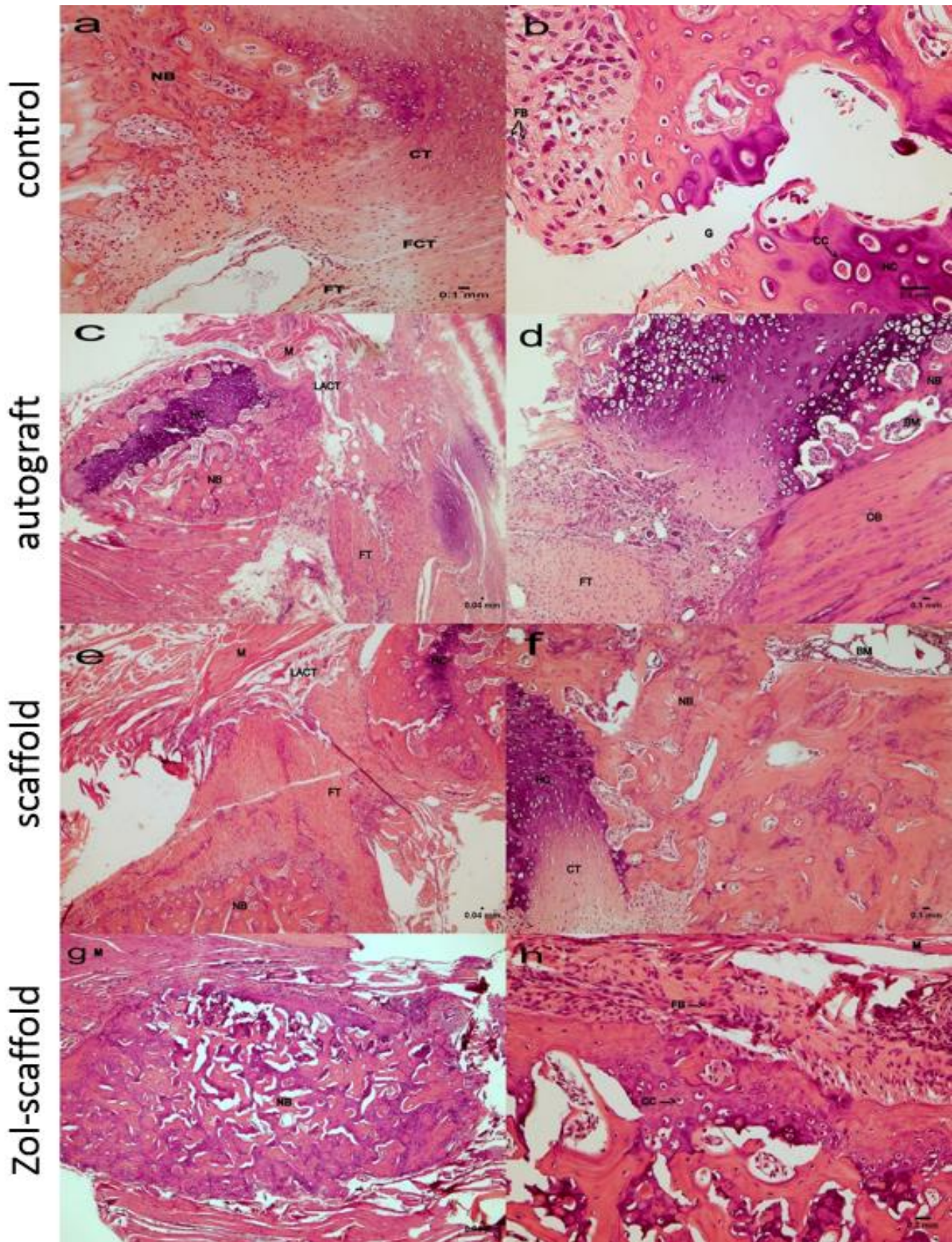
Fig. 7: Histopathology sections from the defect site on the 40th day post-operation. Cartilage tissue was observed in the scaffold group, and fibrous, cartilaginous, and bone-like tissues were seen in the Zol-loaded scaffold group at this stage. The defect region of the non-treated group was filled by fibrous connective tissue. The untreated defect group showed the lowest degree of regeneration. BM: Bone marrow, M: Muscle, NB: New bone, Os: Osteon, FT: Fibrous tissue, FCT: Fibro cartilaginous tissue, CT: Cartilaginous tissue, HC: Hyaline cartilage, OB: Old bone, G: Gap, CC: Chondrocyte, OC: Osteocyte, CB: Chondroblast, and SCR: Scaffold residue
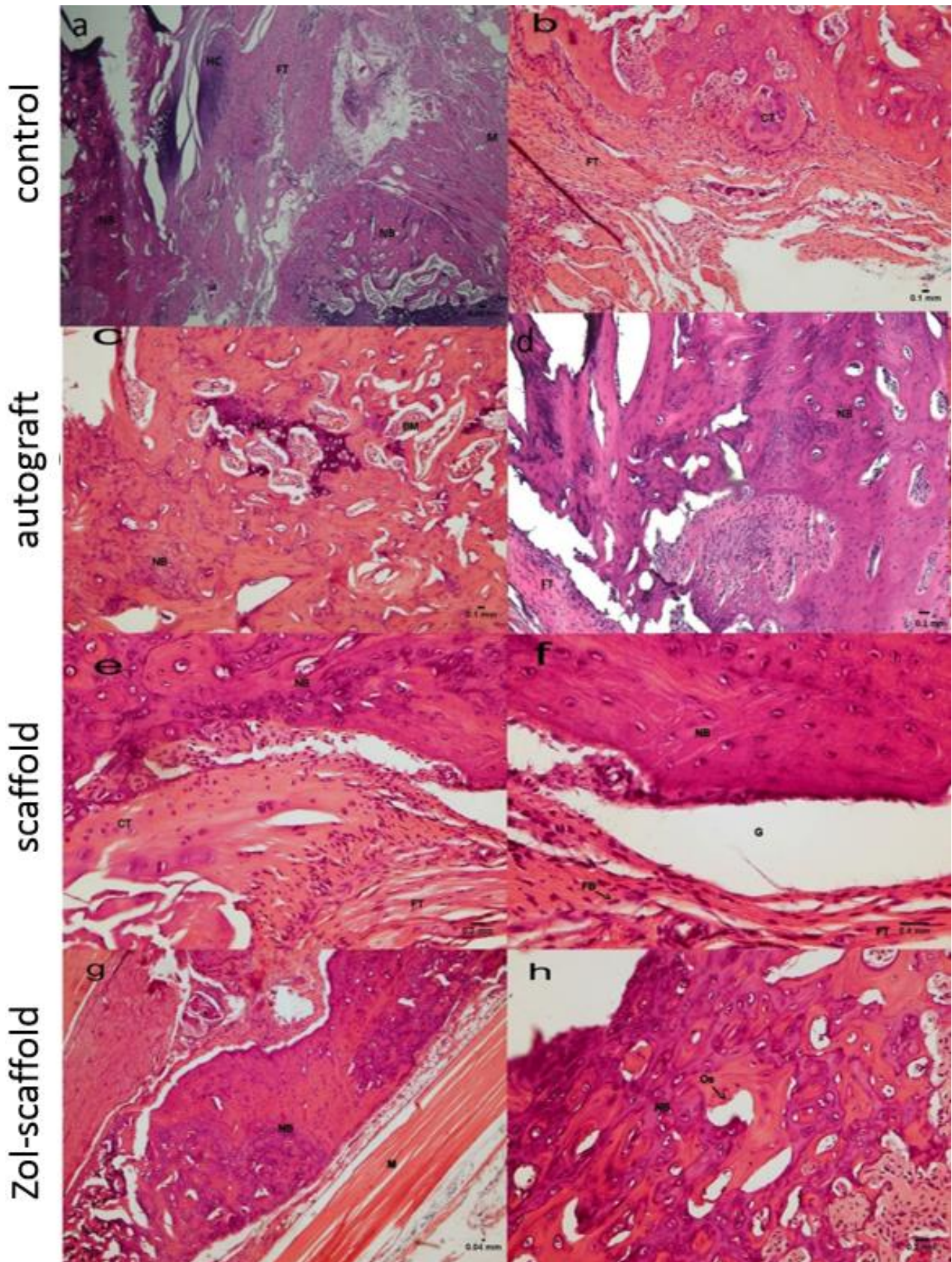
Fig. 8: Histopathology sections of the defect region on the 80th day post-operation. The scaffold was thoroughly degraded and fibrous connective tissue, cartilage, and bone tissue filled the defect area. The autograft and Zol-loaded scaffold groups showed the best results, and their gaps were filled by cartilage and bonny tissues. BM: Bone marrow, M: Muscle, NB: New bone, Os: Osteon, FT: Fibrous tissue, FCT: Fibrocartilaginous tissue, CT: Cartilaginous tissue, HC: Hyaline cartilage, OB: Old bone, G: Gap, CC: Chondrocyte, OC: Osteocyte, CB: Chondroblast, and SCR: Scaffold residue
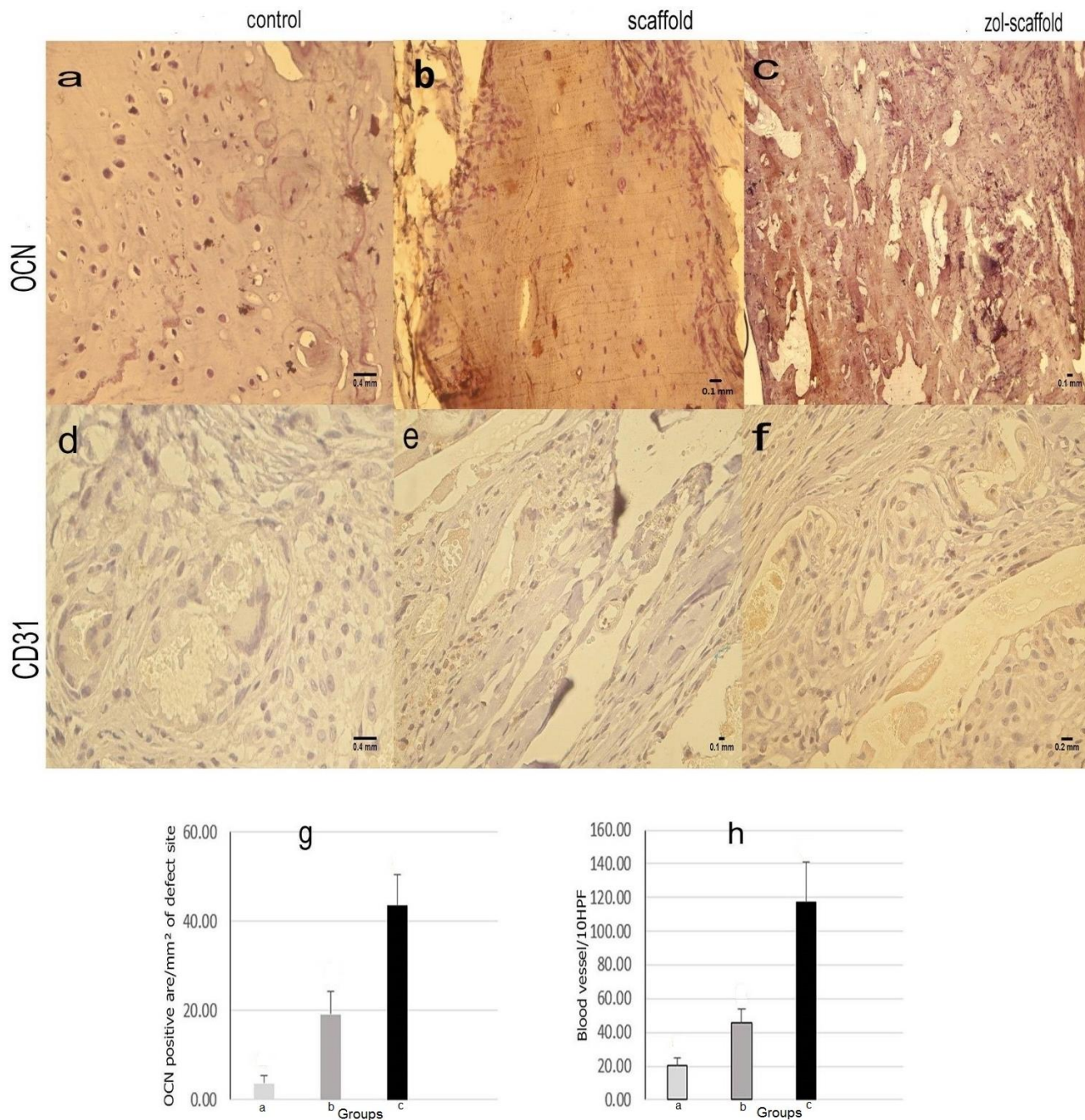
Fig. 9: IHC images of the gap region in the untreated, scaffold, and Zol-loaded scaffold groups based upon the osteogenic and angiogenic markers. The brown color demonstrated positive staining for these markers. a: Untreated, b: PLA/PCL/HA scaffold, and c: Zol-loaded scaffold. *OCN*: a *vs.* b: P<0.01, b *vs.* c: P<0.01, a *vs.* c: P<0.001. *CD31*: a *vs.* b, c: P<0.05

following zero shear viscosity trend demonstrated as PCL>PLA/PCL (50/50)>PLA, indicating that the elasticity of PCL/PLA was promoted after adding the PCL portion and achieved a sufficient elasticity for bone tissue. Factors such as hydrophilicity, porosity, and the microstructure of the mixture had a crucial role in the degradation behavior of this scaffold. In an earlier investigation, a deduction in the pH value occurred due to the presence of the HA particles that released alkaline ions into the solution (Hassanajili *et al*., 2019). By *in vitro* observation of the scaffold degradation, it was concluded that reduction in the degree of degradation was an outcome of the elevated capacity of the scaffold component in the phosphate buffer solution. The FTIR results showed that the PLA and HA chemical interactions led to some shifts in peak positions. As the weight ratio of Ca/P was 1.7, the elemental analysis results suggested that HA adheres at many points of the scaffold (Eshraghi and Das, 2012). The XRD results depicted that the PLA/PCL/HA sample indicated all characteristic peaks after HA addition. HA and PLA interaction led to this change. In fact, this may be due to the subtraction of the PLA crystallinity, and the weak intensity and broadness of this material.
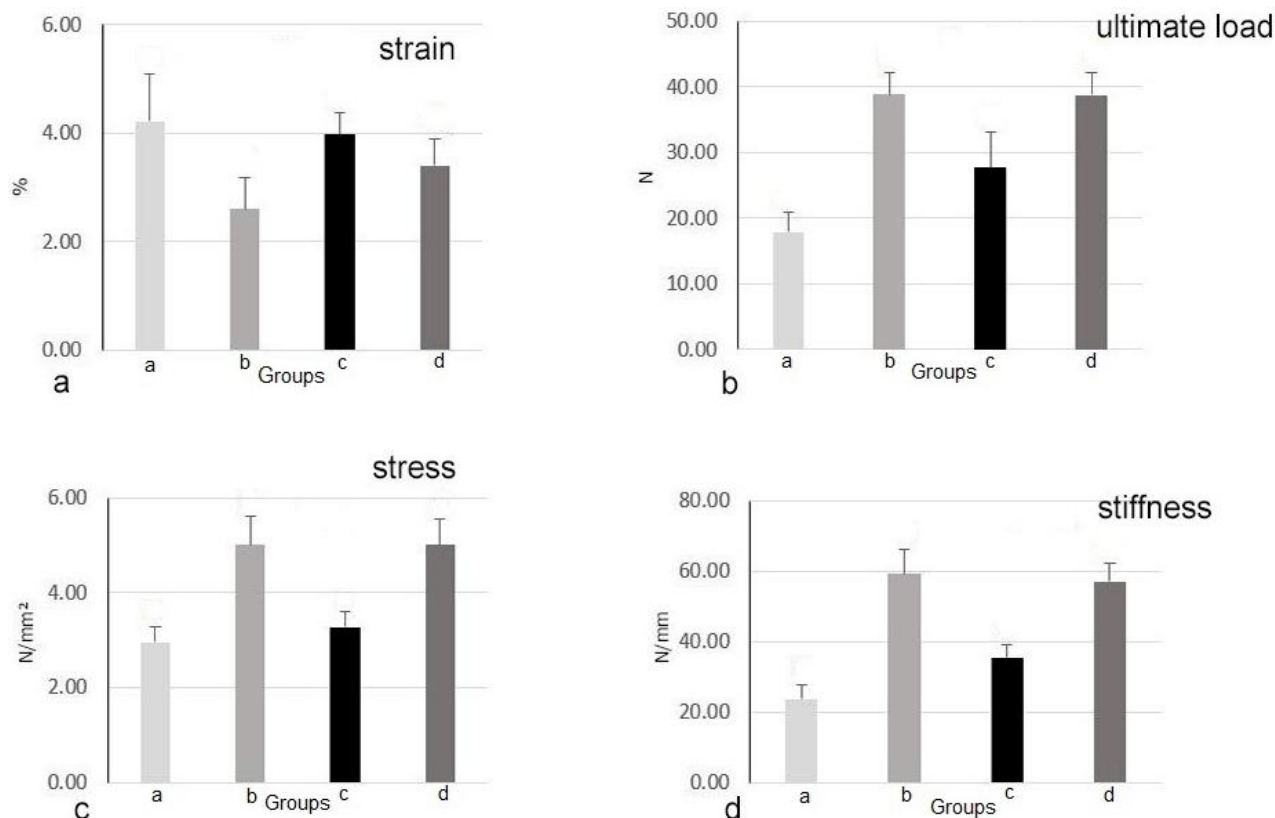
Fig. 10: The biomechanical performance of the scaffold, Zol-loaded scaffold, autograft, and untreated defect on the 80th day post-surgery. a: Control, b: Autograft, c: PLA/PCL/HA scaffold, and d: Zol-loaded scaffold. Strain: P<0.001 (a *vs.* b and d), P<0.01 (a *vs.* c), (c *vs.* b and d). Ultimate load: P<0.05 (a *vs.* c), (c *vs.* b and d), P<0.01 (a *vs.* b and d). Stiffness: P<0.001 (a *vs.* b and d), P<0.01 (a *vs.* c), (c *vs.* b and d). Stress: P<0.01 (a *vs.* b and d), (c *vs.* b and d)

Ismail *et al*. (2022) showed that increasing of the PLA and HA in the combination of PCL, PLA, and HA, resulted in the enhanced mechanical behavior of the final biocomposites. On the other hand, the incorporation of HA resulted in the improvement of the mechanical characteristics of the PLA/PCL/HA scaffold which is an important issue for bone tissue and initiates the migration and proliferation of the stem cells from the surrounding area to the injured site (Ismail *et al*., 2022). Senatov *et al*. (2022) showed that a PLA/PCL/HA that had biocompatibility, hydrophilicity, and a volume porosity of 70% improved the structure and function of the injured trabecular bone. Our previous studies showed that the fabricated PLA/PCL/HA scaffold accompanied by mesenchymal stem cells or differentiated osteogenic cells resulted in enhanced bone regeneration (Oryan *et al*., 2020, 2021; Sahvieh *et al*., 2021).

There are some plausible reasons to select bisphosphonates as an appropriate treatment in bone healing, as their beneficial effects have been previously found on osteoblasts and osteocytes differentiation, and protecting them from apoptosis (Yu *et al*., 2012; Kettenberger *et al*., 2014). There is extensive research suggesting that this family can potentially prevent the loss of bone mass by inhibiting osteoclasts activity (Kyllonen *et al*., 2015). In fact, the previous *in vitro* experiments came up with the finding that the low concentration of this family could stimulate the formation of mineralized bone nodules, and inhibit apoptosis of the osteocytes and osteoblasts (Kettenberger *et al*., 2014). Zoledronate is one of the most powerful drugs in this family that is used for certain targeted processes, such as bone healing and stimulating new bone formation. It has been shown that the local delivery of Zol on peri-implants increased the rate of early bone formation and demonstrated an anti-resorptive effect on bone degeneration (Kettenberger *et al*., 2014).

The effectiveness of PLA/PCL/HA implant on bone healing following its implantation in a critical-sized defect was compared to both the autograft and untreated groups. Based on the *in vivo* results of the current study, it was demonstrated that the Zol-loaded PLA/PCL/HA scaffold enhanced the capacity of bone repair to a significant extent, so that the gap in the Zol-loaded PLA/PCL/HA scaffold and the autologous bone graft groups were replaced by osseous tissue, woven bone, and compact bone formation. Higher expression levels of CD31, OPN, and OC, as assessed by the qRT-PCR analysis, indicated enhanced angiogenesis induction and osteoinductivity in the PLA/PCL/HA scaffold group in comparison to the control group. The biomechanical analysis also demonstrated that there was a significant enhancement in the maximum load in the autograft and the Zol-loaded scaffold groups in comparison to the

control group, on the 80th day post-surgery. Ultimately, based on the histopathology, IHC, histomorphometry, radiology, and CT scans' findings, superior quality and quantity of bone regeneration were observed in the Zol-loaded scaffold group. While these results were comparable to the autograft as the golden standard treatment regimen. Because of the favorable effects of zoledronate on bone healing, it seems that this drug can enhance the quantity and quality of new bone formation and is an ideal therapeutic strategy for promoting bone regeneration. The load-bearing function improves when the new bone tissue is remodeled to compact bone (Henkel *et al*., 2013). Based on the autograft limitation, such as its limited availability for large bone defects and additional surgery (Oryan *et al*., 2014a), the utilization of such osteoinductive and osteoconductive biomaterials is necessary.

Acknowledgements

Conflict of interest

There was no conflict of interest.

References

Alidadi, S; Oryan, A; Bigham-Sadegh, A and Moshiri, A (2017). Comparative study on the healing potential of chitosan, polymethylmethacrylate, and demineralized bone matrix in radial bone defects of rat. Carbohydr. Polym., 166: 236-248.

Babczyk, P; Conzendorf, C; Klose, J; Schulze, M; Harre, K and Tobiasch, E (2014). Stem cells on biomaterials for synthetic grafts to promote vascular healing. J. Clin. Med., 3: 39-87.

Boanini, E; Torricelli, P; Gazzano, M; Bella, ED; Fini, M and Bigi, A (2014). Combined effect of strontium and zoledronate on hydroxyapatite structure and bone cell responses. Biomaterials. 35: 5619-5626.

Chen, CH; Liu, JMJ; Chua, CK; Chou, SM; Shyu, VBH and Chen, JP (2014). Cartilage tissue engineering with silk fibroin scaffolds fabricated by indirect additive manufacturing technology. Materials. 7: 2104-2119.

Do, AV; Khorsand, B; Geary, SM and Salem, AK (2015). 3D printing of scaffolds for tissue regeneration applications. Adv. Healthc Mater., 4: 1742-1762.

Doi, Y; Miyazaki, M; Yoshiiwa, T; Hara, K; Kataoka, M and Tsumura, H (2011). Manipulation of the anabolic and catabolic responses with BMP-2 and zoledronic acid in a rat femoral fracture model. Bone. 49: 777-782.

Eftekhari, H; Jahandideh, A; Asghari, A; Akbarzadeh, A and Hesaraki, S (2018). Histopathological evaluation of polycaprolactone nanocomposite compared with tricalcium phosphate in bone healing. J. Vet. Res., 62: 385-394.

Eshraghi, S and Das, S (2012). Micromechanical finite element modeling and experimental characterization of the compressive mechanical properties of polycaprolactone:

hydroxyapatite composite scaffolds prepared by selective laser sintering for bone tissue engineering. Acta Biomater., 8: 3138-3143.

Fang, J; Li, P; Lu, X; Fang, L; Lu, X and Ren, F (2019). A strong, tough, and osteoconductive hydroxyapatite mineralized polyacrylamide/dextran hydrogel for bone tissue regeneration. Acta Biomater., 1: 503-513.

Frydrych, M and Chen, B (2013). Large three-dimensional poly(glycerol sebacate)-based scaffolds – a freeze-drying preparation approach. J. Mater. Chem. B., 1: 6650-6661.

Gotz, W; Tobiasch, E; Witzleben, S and Schulze, M (2019). Effects of silicon compounds on biomineralization, osteogenesis, and hard tissue formation. Pharmaceutics. 11: 117-143.

Grandi, C; Di Liddo, R; Paganin, P; Lora, S; Dalzoppo, D; Feltri, G; Giraudo, C; Tommasini, M; Conconi, MT and Parnigotto, PP (2016). Porous alginate/poly (ε-caprolactone) scaffolds: preparation, characterization and *in vitro* biological activity. Int. J. Mol. Med., 27: 455-467.

Greenwald, AS; Boden, SD; Goldberg, VM; Khan, Y; Laurencin, CT and Rosier, RN (2011). Bone-graft substitutes: Facts, fictions, and applications. J. Bone Joint Surg. Am., 83-A: 98-103.

Gregor, A; Filova, E; Novak, M; Kronek, J; Chlup, H; Buzgo, M; Blahnova, V; Lukasova, V; Bartos, M; Necas, A and Hosek, J (2017). Designing of PLA scaffolds for bone tissue replacement fabricated by ordinary commercial 3D printer. J. Biol. Eng., 11: 31-51.

Greiner, SH; Whild Emann, B; Back, DA; Alidoust, M; Schwabe, P; Haas, NP and Schmidmaier, G (2008). Local application of zoledronic acid incorporated in a poly (D,L-lactide)-coated implant accelerates fracture healing in rats. Acta Orthop., 79: 717-725.

Hassanajili, SH; Karami-Pour, A; Oryan, A and Talaei-Khozani, T (2019). Preparation and characterization of PLA/PCL/HA composite scaffolds using indirect 3D printing for bone tissue engineering. Mater. Sci. Eng. C., 104: 109960.

Henkel, J; Woodruff, MA; Epari, DR; Steck, R; Glatt, V; Dickinson, IC; Choong, PFM; Schuetz, MA and Hutmacher, DW (2013). Bone regeneration based on tissue engineering conceptions-A 21st century perspective. Bone Res., 1: 216-248.

Ismail, R; Cionita, T; Lai, YL; Fitriyana, DF; Siregar, JP; Bayuseno, AP; Nugraha, FW; Muhamadin, RC; Irawan, AP and Hadi, AE (2022). Characterization of PLA/PCL/green mussel shells hydroxyapatite (HA) biocomposites prepared by chemical blending methods. Materials. 15: 8641.

Kettenberger, U; Ston, J; Thein, E; Procter, P and Pioletti, DP (2014). Does locally delivered Zoledronate influence peri-implant bone formation? -Spatio-temporal monitoring of bone remodeling *in vivo*. Biomaterials. 35: 9995-10006.

Kumar, P; Dehiya, BS and Sindhu, A (2018). Bioceramics for hard tissue engineering applications: A review. Int. J. Appl. Eng. Res., 13: 2744-2752.

Kyllonen, L; DEste, M; Alini, M and Eglin, D (2015). Local drug delivery for enhancing fracture healing in osteoporotic bone. Acta Biomater., 11: 412-434.

Lim, SS; Lee, B; Kim, IS and Hwang, SJ (2017). Differential modulation of zoledronate and etidronate in osseous healing of an extracted socket and tibia defect. Oral Surg. Oral Med. Oral Pathol. Oral Radiol., 123: 8-19.

Lopes, MS; Jardini, AL and Maciel, R (2012). Poly (lactic acid) production for tissue engineering applications. Procedia Eng., 42: 1402-1413.

Ma, JH; Guo, WS; Li, ZR and Wang, BL (2018). Local

administration of bisphosphonate-soaked hydroxyapatite for the treatment of osteonecrosis of the femoral head in rabbit. Chin. Med. J., 129: 2559-2566.

Mathavan, N; Bosemark, P; Isaksson, H and Tägil, M (2013). Investigating the synergistic efficacy of BMP-7 and zoledronate on bone allografts using an open rat osteotomy model. Bone. 56: 440-448.

Matos, MA; Tannuri, U and Guarniero, R (2010). The effect of zoledronate during bone healing. J. Orthop. Traumatol., 11: 7-12.

Mondal, D; Griffith, M and Venkatraman, SS (2016). Polycaprolactone-based biomaterials for tissue engineering and drug delivery: Current scenario and challenges. Int. J. Polym. Mater. Polym. Biomater., 65: 255-265.

Moshiri, A; Oryan, A and Shahrezaee, M (2015). An overview on bone tissue engineering and regenerative medicine: current challenges, future directions and strategies. J. Sports Med. Doping Stud., 5: e144.

Ortega, AJ; Campbell, PM; Hinton, R; Naidu, A and Buschang, PH (2012). Local application of zoledronate for maximum anchorage during space closure. Am. J. Orthod. Dentofacial Orthop., 1426: 780-791.

Oryan, A; Alidadi, S; Bigham-Sadegh, A and Moshiri, A (2017). Effectiveness of tissue engineered based platelet gel embedded chitosan scaffold on experimentally induced critical sized segmental bone defect model in rat. Injury. 48: 1466-1474.

Oryan, A; Alidadi, S; Moshiri, A and Maffulli, N (2014a). Bone regenerative medicine: Classic options, novel strategies, and future directions. J. Orthop. Surg. Res., 9: 18.

Oryan, A; Bigham-Sadegh, A and Abbasi-Teshnizi, F (2014b). Effects of osteogenic medium on healing of the experimental critical bone defect in a rabbit model. Bone. 63: 53-60.

Oryan, A; Hassanajili, S and Sahvieh, S (2021). Effectiveness of a biodegradable 3D polylactic acid/poly (ε-caprolactone)/hydroxyapatite scaffold loaded by differentiated osteogenic cells in a critical-sized radius bone defect in rat. J. Tissue Eng. Reg. Med., 15: 150-162.

Oryan, A; Hassanajili, S; Sahvieh, S and Azarpira, N (2020). Effectiveness of mesenchymal stem cell-seeded onto the 3D Polylactic acid/Polycaprolactone/ Hydroxyapatite scaffold on the radius bone defect in rat. Life Sci., 257: 118038.

Oryan, A; Meimandi-Parizi, A; Shafiei-Sarvestani, Z and Bigham, AS (2012). Effects of combined hydroxyapatite and human platelet rich plasma on bone healing in rabbit model: radiological, macroscopical, histopathological and biomechanical evaluation. Cell Tissue Bank. 13: 639-651.

Ottensmeyer, P; Witzler, M; Schulze, M and Tobiasch, E (2018). Small molecules enhance scaffold-based bone grafts via purinergic receptor signaling in stem cells. Int. J. Mol., 19: 3601-3630.

Roshan-Ghias, A; Arnoldi, J; Procter, P and Pioletti, DP (2011). *In vivo* assessment of local effects after application of bone screws delivering bisphosphonates into a compromised cancellous bone site. Clin. Biomech., 26: 1039-1043.

Sahvieh, S; Oryan, A; Hassanajili, S and Kamali, A (2021). Role of bone stem cell-seeded 3D polylactic acid/ polycaprolactone/hydroxyapatite scaffold on a critical-sized radial bone defect in rat. Cell Tissue Res., 383: 735-750.

Senatov, F; Zimina, A; Chubrik, A; Kolesnikov, E; Permyakova, E; Voronin, A; Poponova, M; Orlova, P; Grunina, T; Nikitin, K; Krivozubov, M; Strukova, N; Generalova, M; Ryazanova, A; Manskikh, V; Lunin, V; Gromov, A and Karyagina, A (2022). Effect of recombinant BMP-2 and erythropoietin on osteogenic properties of biomimetic PLA/PCL/HA and PHB/HA scaffolds in critical-size cranial defects model. Biomater. Adv., 135: 112680.

Senel, FC; Duman, MK; Muci, E; Cankaya, M; Pampu, AA; Ersoz, S and Gunhan, O (2010). Jaw bone changes in rats after treatment with zoledronate and pamidronate. Oral Surg. Oral Med. Oral Pathol. Oral Radiol. Endod., 109: 385-391.

Shahsavari-Pour, S; Aliabadi, E; Latifi, M; Zareifard, N; Namavar, MR and Talaei-Khozani, T (2018). Evaluation of the possible synergic regenerative effects of platelet-rich plasma and hydroxyapatite/zirconia in the rabbit mandible defect model. Iran J. Med. Sci., 43: 633-644.

Washington, KE; Kularatne, RN; Karmegam, V; Biewer, MC and Stefan, MC (2017). Recent advances in aliphatic polyesters for drug delivery applications. Wiley Interdiscip. Rev. Nanomed. Nanobiotechnol., 9: e1446.

Witzler, M; Ottensmeyer, PF; Gericke, M; Heinze, T; Tobiasch, E and Schulze, M (2019). Non-cytotoxic agarose/hydroxyapatite composite scaffolds for drug release. Int. J. Mol. Sc., 20: 35-65.

Yu, W; Li, R; Long, J; Chen, P; Hou, A; Li, L; Sun, X; Zheng, G; Meng, H; Wang, Y; Wang, A; Sui, X; Guo, Q; Tao, S; Peng, J; Qin, L; Lu, S and Lai, Y (2019). Use of a three-dimensional printed polylactide-coglycolide/ tricalcium phosphate composite scaffold incorporating magnesium powder to enhance bone defect repair in rabbits. J. Orthop. Translat., 16: 62-70.

Yu, YY; Lieu, S; Hu, D; Miclau, T and Colnot, C (2012). Site specific effects of zoledronic acid during tibial and mandibular fracture repair. PLoS One. 7: e31771.